Available online at www.scholarsresearchlibrary.com

Scholars Research Library

Archives of Physics Research, 2012, 3 (2):116-122
(http://scholarsresearchlibrary.com/archive.html)

Scholars Research Library
ISSN : 0976-0970
CODEN (USA): APRRC7

Development of In^{3+} substituted Mn-Ni-Zn nanoferrite core material

Suresh R. Kulkarni

Department of Physics, Rajaram College, Kolhapur (India)

ABSTRACT

Nanostructured Mn-Ni-Zn ferrite with composition $Mn_{0.1}Ni_{0.6}Zn_{0.3}In_xFe_{(2-x)}O_4$ (x =0.05, 0.1, 0.15, 0.2) was prepared by sol-gel method. X-ray diffraction (XRD) patterns of all samples showed the spinel structure. The dielectric permeability, AC resistivity and DC resistivity was measured and it was observed that the sample with x = 0.1 has highest resistivity. Vibrating Sample Magnetometry (VSM) is used to characterize the magnetic properties of prepared nanoferrites. The maximum saturation magnetization (36.2 emu/g) was observed for the sample with x = 0.1. For the same sample the coercivity was found very small (7 Oe). These materials are expected to have applications in core material and in electronic devices technology.

Keywords: Nanoferrites, Sol-gel method, Dielectric loss, Saturation magnetization.

INTRODUCTION

The bulk properties of ferrites changes as its dimensions are changed to nanoscale. With the improvement in the synthesis and characterization techniques, there is tremendous growth in the field of ferrites. Superparamagnetism, spin canting, core-shell structure, metastable cation distribution etc are some of the phenomena, which have been observed in various nanoferrites. These phenomena depend on number of factors such as composition, grain size, surface morphology, anisotropy, interparticle interactions. Mn-Ni-Zn nanoferrites are of great importance from the point of view of scientific and industrial applications. These ferrites are used in high frequency applications as transformer cores, antenna rods, rf coils, radar absorbing material etc. The usual synthesis of ferrite materials, a ceramic method is used in which the particle size increases due to heating at high temperature for long time. The chemical methods are useful to obtain high homogeneity of phases, fine particle size and high magnetic characteristics [1].

Nanoparticles of spinel ferrites have been investigated in recent years for their usual electrical and magnetic properties and applications in information storage systems, magnetic bulk cores, microwave absorbers and medical diagnostics. The synthesis and characterization of superparamagnetic nanoparticles of spinel ferrites with the chemical formula MFe_2O_4 (M=Co, Mn, Ni, Zn, Mg etc) have been investigated with much interest. Nano size effect and the large surface area of nanoparticles dramatically change the magnetic properties and exhibit superparamagnetism, because each particle can be considered as single magnetic domain [2].

This research work communicates the electrical and magnetic properties of In^{3+} ion substituted Mn-Ni-Zn nanoferrites. The choice of this system is made so as to yield large electrical resistivity and high saturation magnetization. These ferrites are synthesized by sol-gel method so as to control the micro structural properties such as grain size, distribution and orientation easily.

MATERIALS AND METHODS

2.1 Synthesis of Nanoferrites:

$Mn_{0.1}Ni_{0.6}Zn_{0.3}In_xFe_{(2-x)}O_4$ (x =0.05, 0.1, 0.15, 0.2) nanoferrites were prepared by sol-gel method. A 10 % of polyvinyl alcohol (PVA) solution was prepared by dissolving 10 g of solid PVA in 100 ml of distilled water. The mixture was stirred well using magnetic stirrer for 30 minutes at 80^{o}C. The molar quantity of AR grade metal nitrates $Mn(NO_3)_2$, $Zn(NO_3)_2$, $Ni(NO_3)_2$, $In(NO_3)_3$ and $Fe_2(NO_3)_2$ were taken as starting material. These nitrates were dissolved separately in 10 ml of distilled water and stirred well for 30 minutes at 80^{o}C. These aqueous solutions were mixed in a beaker and stirred for 30 minutes at 80^{o}C to prepare precursor solution. The aqueous solution of PVA in measured quantities was added by drop to the precursor solution and dehydrated around 150^{o}C under continuous stirring to get a red gel type product. The gelation was continued to release of reddish brown fumes around 400^{o}C, the gel further got converted into a fluffy ferrite mass. The prepared ferrite mass was pressed in the form of pellets of 1.5 cm diameter with the help of hydraulic press by applying pressure of 7 tonnes/sq. inch for 10 minutes. These pellets were sintered at 500^{o}C for 4 hours in air medium.

2.2 Characterization

X- ray diffraction (XRD) pattern was carried out on a X- ray diffractometer, Model Bruker D8 Advance Diffractometer with CuKα irradiation (λ = 1.5405 Å). The lattice parameter, crystallite size and porosity of the prepared samples were calculated from the XRD data. The Scanning Electron Microscopy (SEM) (JEOL JSM-6360A microscope) was used to study the morphology of the prepared samples. The dielectric permeability and loss factor (tanδ) were measured by two probe method using LCR meter bridge (HP 4284 A) in the frequency range of 100 Hz to 1 MHz at room temperature. The ac resistivity (ρ_{ac}) was calculated from the dielectric data and loss tangent. The dc resistivity was measured by conventional method by applying a suitable voltage across the pellet and the resultant current was measured. Vibrating Sample Magnetometer (VSM) was employed to study the magnetic properties of the samples in the field of 7 kOe at room temperature.

RESULTS AND DISCUSSION

3.1 Structural analysis

XRD patterns have confirmed the spinel structure in all samples. Fig. 1 shows XRD patterns of $Mn_{0.1}Ni_{0.6}Zn_{0.3}In_xFe_{(2-x)}O_4$ (x =0.05, 0.1, 0.15, 0.2) prepared by sol-gel method. The peak position and relative intensity of all diffraction peaks was match well with the standard powder diffraction data and no impurity peaks were observed. The broad XRD lines indicate that the ferrite particles are nanosize. The average crystallite size for each composition was calculated from the XRD line width of the (311) peak using Scherrer formula. The values of crystallite size and lattice constant deduced from the X-ray data are given in the Table.1. The substitution of In^{3+} ions, the lattice parameter was found to increase with increasing concentration of substituted ions and this change was observed from 8.382 to 8.457. The observed lattice parameter and specific indices are characteristic of spinel structure confirms the formation of cubic spinel structure in ferrite [3, 4]. The patterns do not show any unidentified peaks confirming no diffusion or any chemical reaction during sintering [5].

The percentage porosity of these samples was measured using the following formula:

$$\text{Percentage porosity} = \left(\frac{\rho_x - \rho_a}{\rho_x} \right) \times 100 \qquad \ldots(1)$$

where, ρ_x is the x-ray density and ρ_a is the bulk density. The value of ρ_x for ferrite was calculated using the formula

$$\rho_{x\ (Ferrite)} = 8M / Na^3 \qquad \ldots(2)$$

where, M is the molecular weight expressed in grams, a is the lattice constant and N is the Avogadro's number = 6.023×10^{23}.

It was observed that the porosity increases from 11.54 % to 12.36 % with the substitution of In^{3+} ions. The porosity of ceramic samples results from two sources, intragranular porosity and intergranular porosity [6]. The total porosity is the sum of these two porosities. It was reported that the intergranular porosity depends on the crystallite size.

From the crystallite size data, there is variation in crystallite size 15.03 nm to 27.78 nm for In^{3+} substituted samples. Therefore the total porosity is mainly due to intergranular porosity [7].

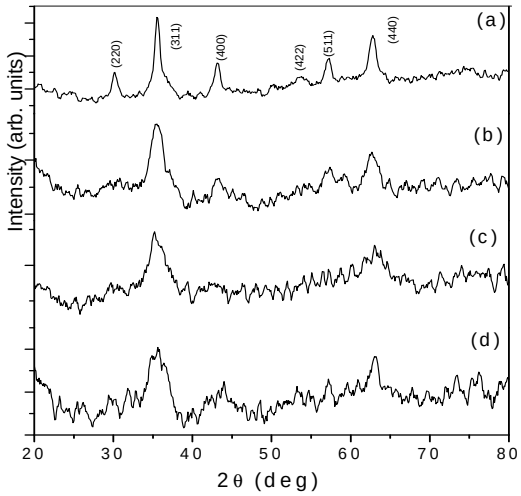

Fig.1

Fig. 2 shows the SEM image of $Mn_{0.1}Ni_{0.6}Zn_{0.3}In_xFe_{(2-x)}O_4$ with x = 0.1. It was seen that the large number of nanoparticles collect into a mass (agglomeration) and therefore if these samples scanned at higher magnification, fine nanoparticles could be viewed. The crystallite size calculated by Scherrer formula using full-width half maximum (FWHM) of (311) XRD peak show nano size of particles.

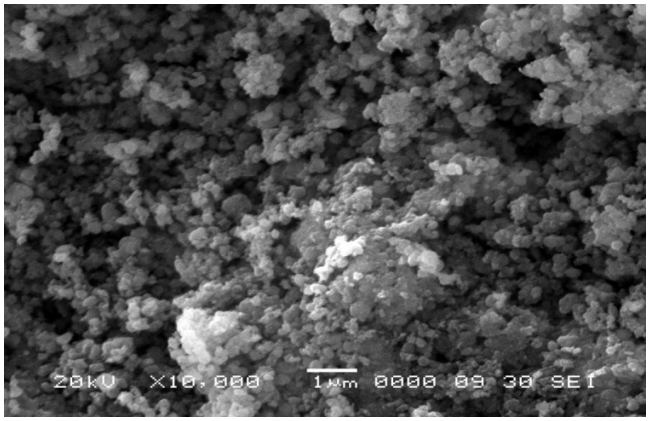

Fig.2 SEM of $Mn_{0.1}Ni_{0.6}Zn_{0.3}In_xFe_{2-x}O_4$ with x=0.1

3.2 Electrical properties

The dielectric constant (ϵ') was calculated using the formula:

$$\epsilon' = C_p.t / \epsilon_o A \qquad \ldots (2)$$

where, C_p is the capacitance of the pellet in farad, t is the thickness of pellet in meter, r is the radius of cross-section of the pellet in meter and ϵ_o is the permittivity of free space. Fig. 3 shows the variation of dielectric constant ϵ' with frequency for all the samples. The dielectric constant ϵ' decreases with increase in frequency showing the dispersion in a certain range of frequency and it remains constant at higher frequencies. The large value of ϵ' at

lower frequency has been attributed to the effect of heterogeneity of the samples [8]. The dielectric dispersion is due to interfacial polarization in agreement with Koop's phenomenological theory [9]. The exchange of 3d electrons between Fe^{3+} and Fe^{2+} which are localized at the metal ions, results in local displacement of electrons in the direction of field which determines the strength of polarization. The low value of dielectric constant was observed for the sample $Mn_{0.1}Ni_{0.6}Zn_{0.3}In_xFe_{2-x}O_4$ with x =0.1. This low value is attributed to the method of synthesis (sol-gel method) which suppresses the formation of Fe^{2+} ions. At low frequency, the tan δ value

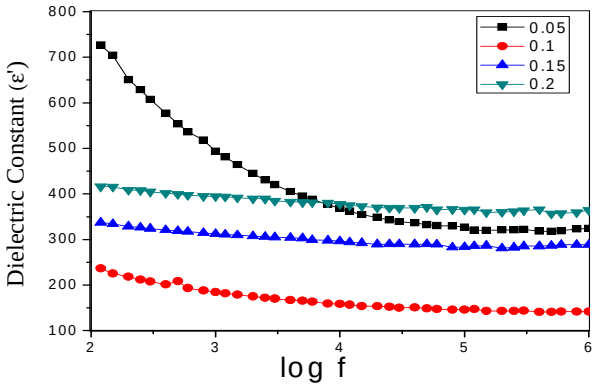

Fig. 3 Variation of dielectric constant with frequency for $Mn_{0.1}Ni_{0.6}Zn_{0.3}In_xFe_{2-x}O_4$ (x = 0.05 to 0.2)

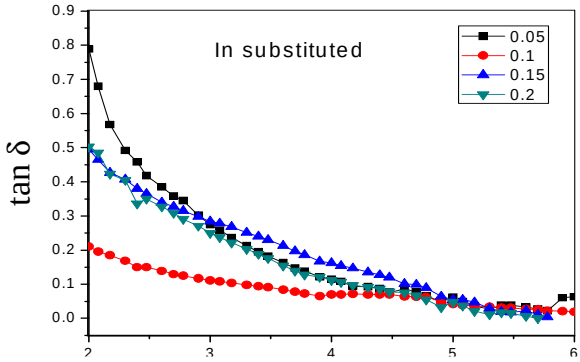

Fig. 4 Variation of loss tangent with frequency for $Mn_{0.1}Ni_{0.6}Zn_{0.3}In_xFe_{2-x}O_4$ (x = 0.05 to 0.2)

was observed to be large and it decreases with increasing frequency (Fig.4). The physical significance of tan δ is the energy dissipation in the dielectric system. In the higher frequency range, the loss vanishes and the dipole orientation contributes to the polarization. The ac resistivity ρ_{ac} was calculated from dielectric data and loss tangent using the relation.

$$\rho_{ac} = 1/(\epsilon' \epsilon_o \omega \tan \delta) \qquad \ldots (3)$$

where, ω is the angular frequency, tan δ is a loss factor and ϵ' is a real part dielectric constant. In $Mn_{0.1}Ni_{0.6}Zn_{0.3}In_xFe_{2-x}O_4$, the AC resistivity was observed to be increases with the substitution of In upto x = 0.1 and then decreases for the samples x > 0.1. The highest value of AC resistivity (1.083 $x10^8$ V-cm) was observed for In substituted nanoferrites (Fig.5). The observed values are much higher than those reported in the literature for Ni-Zn ferrites prepared by the ceramic method [10]. The conduction in ferrites is reported to be due to hopping of electrons on application of electric field. The increase of Fe^{2+} concentration in the sample increases the hopping probability resulting in decease of resistivity at higher frequencies [11].

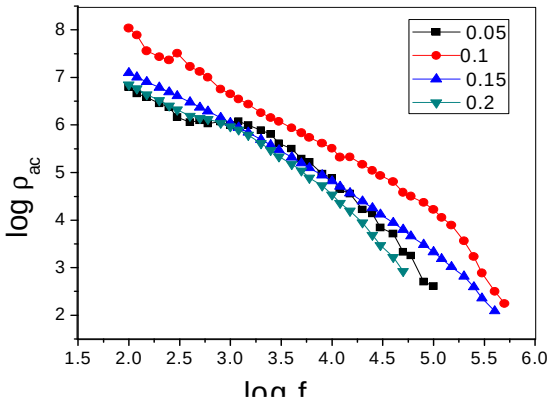

Fig. 5 Variation of ac resistivity with frequency for $Mn_{0.1}Ni_{0.6}Zn_{0.3}In_xFe_{2-x}O_4$ (x = 0.05 to 0.2)

The variation of dc resistivity with temperature for all ferrites is shown in Fig. 6. In $Mn_{0.1}Ni_{0.6}Zn_{0.3}In_xFe_{2-x}O_4$ ferrites, the resistivity initially reduces with very little rate upto 500 K and thereafter decreases linearly with temperature. The maximum value ρ_{dc} (9.468 x10^7) was observed for the sample with x =0.1. A break in the linear variation of resistivity was observed at their respective Curie temperature (Table 1). There is change in activation energy when the sample undergoes ferromagnetic to paramagnetic phase transition. The activation energies (ΔE) calculated in the ferromagnetic transition region was observed greater than in paramagnetic region. This increase in the activation energy was attributed to the volume expansion during the magnetic transition from order-disorder state [12]. Similar results were reported for Ni-Zn ferrites [13] and it suggests that the conduction mechanism in these ferrites is predominantly due to hopping of electrons. A reasonable value of resistivity for all samples at room temperature was observed than that of earlier reports. The improvement in electrical resistivity is attributed to the large number of ultra fine grains with much number of grain boundaries.

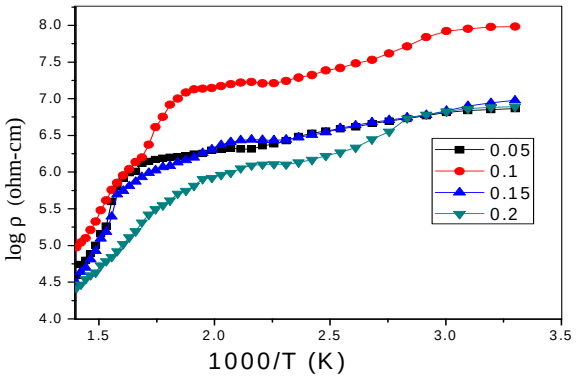

Fig. 6 Variation of DC resistivity with temperature for $Mn_{0.1}Ni_{0.6}Zn_{0.3}In_xFe_{2-x}O_4$ (x = 0.05 to 0.2)

3.3 Magnetic properties

The value of magnetization sharply increases with the field strength in the low field region. However, it could not reach the saturation state even in the presence of strong magnetic field 7 kOe.(Fig.7) Similar observations at room temperature magnetization have been reported by others [14,15]. For all samples, a superparamagnetic 'S' like shape hysteresis curves were observed. The saturation magnetization M_s of the samples were found by extrapolating M_s vs 1/H plot to 1/H=0. It was observed that the value of M_s was maximum (36.2 emu/g) for the

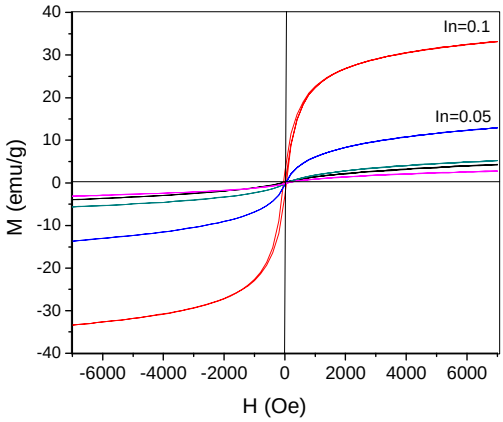

Fig.7 Magnetic hysteresis loops of $Mn_{0.1}Ni_{0.6}Zn_{0.3}In_xFe_{2-x}O_4$ (x=0.05 to 0.2) nanoferrites

sample x = 0.1. The saturation magnetization decreases for the samples with x>0.1. This decrease of saturation magnetization can be explained on the basis of cation distribution. As the In concentration increases, the magnetization of B site (M_B) decreases while that of A site (M_A) increases. Therefore the net magnetization (M_B-M_A) decreases [16]. However these values are low for all compositions than their corresponding values for bulk ferrites. The reduction of M_s in nanoparticles is attributed to the existence of random canting of particles caused by antiferromagnetic exchange interactions due to asymmetry of these spins [17]. The low value of coercivity indicates that the transformation from ferromagnetic to superparamagnetic behavior. In the superparamagnetic state of the material, the room temperature thermal energy overcomes the magnetostatic energy, resulting in zero hysteresis. In other words, the particle itself is a single domain ferromagnet having ability to store magnetization information [18].

Table 1: The values of lattice parameter, crystallite size, % porosity, AC/DC resistivity, saturation magnetization (M_s) and coercivity (H_c) of $Mn_{0.1}Ni_{0.6}Zn_{0.3}Al_xFe_{2-x}O_4$ nanoferrites

Composition X	Lattice parameter (Å)	Crystallite size (nm)	% porosity	$(\rho_{ac})_{max}$	$(\rho_{dc})_{max}$	M_s (emu/g)	H_c (Oe)
0.05	8.382	22.12	12.36	6.197×10^6	7.320×10^6	14.2	10
0.10	8.407	15.03	11.97	1.083×10^8	9.468×10^7	36.2	7
0.15	8.427	19.72	11.97	1.246×10^7	9.470×10^6	7.7	14
0.20	8.457	27.78	11.54	7.002×10^6	7.811×10^6	4.7	18

CONCLUSION

i) The broad XRD lines indicate that the ferrite particles are nanosize. The observed lattice parameter and specific indices are characteristic of spinel structure.
ii) The low value of dielectric constant is attributed to the method of synthesis (sol-gel method) which suppresses the formation of Fe^{2+} ions. The value of tan δ for these samples is very small at higher frequencies up to 100 kHz.
iii) The higher values of DC resistivity are attributed to the increase of intergranular porosity which hinders the motion of charge carriers. The higher values of AC resistivity for these ferrites indicate that these ferrites can be used in the application at higher frequencies.
iv) For all samples, a superparamagnetic 'S' like shape hysteresis curves were observed. The value of M_s increases with In doping up to x = 0.1 and then decreases rapidly.
The prepared ferrite materials have high DC resistivity, high AC resistivity, very low dielectric loss and high saturation magnetization. These results are promising for the use of these materials in high frequency applications.

Acknowledgements
This work is supported by University Grants Commission under the scheme of financial assistance to college teachers for undertaking Minor Research Project.

REFERENCES

[1] Y-P Fu, C-H Lin, *J. Magn. Magn. Mater*. **2002,** 251, 74.
[2] D. S. Mathew, R. S. Juang, *J. Chem. Engg*. **2007,** 139, 51-65.
[3] B.D. Cullity, "Elements of X-ray diffraction" Addison-Wesley Publish. Co., England **1967,** 42.
[4] L. V. Azaroff, "Elements of x-ray crystallography" Mc-Graw Hill, New York ,**1974,**220.
[5] Atul Thakur, P. Mathur, M. Singh, *Ind. J. Pure & Appl. Phy*. **2008,** 46 43.
[6] W. D. Kingery, H. K. Biwen, D. R. Uhlmann, Introduction to Ceramics, John Willey and sons, New York. **1975,** 458.
[7] A. A. Sattar, H. M. El-Sayed, K. M. El-Shokrofy, M. M. El-Tabey,*J. Appl. Sci*. **2005,** 5, 164.
[8] R. P. Mahajan, K. K. Patankar, N. M. Burange, S. C. Chaudhari, A. K. Ghatage and S. A. Patil, *Indian. J. Pure and Appl. Phys*., **2000,** 38, 615-620
[9] S. L. Kadam, K. K. Patankar, C. M. Kanamadi, B. K. Chougule *Mater. Res. Bull*., **2004,** 39, 2265-2272
[10] M. B. Kothale, K. K. Patankar, S. L. Kadam, V. L. Mathe, A. V. Rao and B. K. Chougule, *Mater. Chem. and Phys*. **2002,** 72, 691
[11] L. S. Deshmukh, K. Krishnakumar, S. Balakshan, A. Ramkrishna and G. Sasathaiah, *Bull. Mater. Sci*., **1998,** 21(5), 723.
[12] A. K. Singh, A. Verma, O. P. Thakur, R. G. Mendiratta, *Mater. Lett*. **2003,** 57, 1041.
[13] J. Smit, H. P. J. Wijn, Ferrites, Philips Technical Library, Netherland **1959,**150.
[14] A. A. Sattar, H. M. El-Sayed, M. M. El-Tabey, *J. Mater. Sci*. **2005,** 40 , 4873.
[15] H. M. El-Sayed, *Am. J. Appl. Sci*. **2006,** 3 (10), 2035.
[16] Y. Koseoglu, A. Baykal, *Polyhedorn* **2009,** 28, 2887-2892.
[17] J. Wang, *J. Magn. Magn. Mater*. **2007,** 309, 295.
[18] H. Xue, Z. Li, X. Wang, *Mater. Lett*. , **2007**, 61,347.